Band-gap narrowing and band structure in degenerate tin oxide (SnO_2) films

Geeta Sanon, Raj Rup, and Abhai Mansingh
Department of Physics and Astrophysics, University of Delhi, Delhi 110 007, India
(Received 4 December 1990; revised manuscript received 22 April 1991)

Films of tin oxide (SnO_2) were deposited on a quartz substrate by the chemical-vapor-deposition technique. Carrier densities in the range 6.1×10^{19}–1.3×10^{21} cm^{-3} were obtained by varying the thickness from 0.20 to 1.55 μm. The transmittance and reflectance were measured in the wavelength range 0.2–0.9 μm. The band gap as well as the transition width were found to increase with increasing carrier density. The present data, along with the results reported for SnO_2 films by some other workers, have been analyzed by taking into account the narrowing, which is due to electron-electron and electron-impurity scattering, and the Burstein-Moss widening, which is due to the filled lower states in the conduction band. Experiment and theory are reconciled by assuming a valence-band effective mass $\sim 1.0m_0$. Adding the narrowing for different carrier densities to the observed widening at respective concentrations gives the actual Burstein-Moss widening. Other reported data for SnO_2 films can be fit very well to the present effective-mass values. However, the intrinsic band gap E_{g0} works out to be different for different workers and seems to be a function of deposition conditions. It is also shown that the narrowing at the center of the band is much higher than that corresponding to the Fermi wave number and the difference increases with n_e. A distortion in the shape of the bands is thereby expected at high carrier densities.

INTRODUCTION

The fundamental absorption region of degenerate oxide semiconductors, viz., ZnO, In_2O_3, indium tin oxide, and SnO_2, has become the subject of interest for many researchers in the recent past. Having a unique combination of electrical and optical properties, these materials find a wide range of applications as transparent electrodes in various electro-optical devices and as heat mirrors in solar collectors.[1–4] Until recently, the research on these materials was confined to achieving a high transparency in the visible region and high reflectivity in the infrared region, besides good electrical conductivity. There are a large number of papers on indium tin oxide, In_2O_3, ZnO, and SnO_2 in which the shift of the fundamental absorption edge to higher frequencies with increasing carrier density has been pointed out.[5–15] However, such a shift of the band gap has been attributed solely to the Burstein-Moss (BM) effect[16] by most of them. It is only after detailed theoretical studies of the band-gap shifts in heavily doped semiconductors such as Si, Ge, and GaAs,[17–19] that the importance of the contribution of the many-body interactions to the band-gap shifts has been realized. The above studies suggest that, above the Mott critical density,[20] the widening of the band gap due to the BM shift is always accompanied by a band-gap narrowing which is caused by the lowering of the conduction band and an upward shift of the valence band on account of the electron-electron and electron-impurity interactions. Working along similar lines, Hamberg *et al.*[21] showed that neglecting the narrowing leads to a negative valence-band effective mass for indium tin oxide. This would imply that the valence band is curved in the same direction as the conduction band. This ambiguity could, however, be removed by taking into account the self-energies due to many-body interactions. Jin *et al.*[22] again followed the same model for ZnO films and obtained a positive valence-band effective mass.

To the best of our knowledge, the narrowing of the band gap in tin-oxide (SnO_2) films has not been taken into account by any worker so far. Moreover, though a conduction-band effective mass has been reported to lie somewhere between $0.1m_0$ and $0.8m_0$ by a few workers,[23–29] little has been said about the valence-band effective mass. Shanthi *et al.*[26] have reported a negative valence-band effective mass for SnO_2 films. In the present paper, we wish to extend the model given by Berggren and Sernelius,[17] to tin-oxide films. An attempt has been made to analyze the optical properties of the degenerate SnO_2 films by taking into account both the widening and the narrowing of the band gap. It is shown that the contribution of the self-energy terms to the band-gap shift is significant. The effect of the degree of degeneracy on the shapes of the bands has also been discussed.

I. EXPERIMENT

Thin films of SnO_2 are deposited on glass and quartz substrate, by the chemical-vapor-deposition technique. Nitrogen gas is used to carry the reactants kept in separate bubblers. The heterogeneous reaction involved is

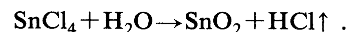

$$SnCl_4 + H_2O \rightarrow SnO_2 + HCl\uparrow \ .$$

The detailed preparation technique is described elsewhere.[30]

For the present studies, only the samples deposited on quartz substrate have been used to ensure that the absorption edge of the substrate in the uv region is at a higher frequency than that of the samples. In order to

©1991 The American Physical Society

study the band-gap shift with carrier concentration, samples of different degrees of degeneracy were required. A change in the carrier density could be obtained by varying the deposition temperature,[31] introducing suitable dopants, e.g., Sb and F,[14–26] annealing the film in different ambients,[15,32] and by varying the thickness.[33–35] The theory involving the change in the band gap due to a change in carrier density assumes a constant value of the intrinsic band gap (E_{g_0}). However, it has been observed by many workers that the value of E_{g_0} of a given material depends on the deposition conditions.[21,35] Of all the above-mentioned methods of varying the carrier concentration, we have utilized the last one, namely, the variation of carrier concentration with thickness where all deposition parameters except the duration of deposition are kept fixed. It is observed that the grain size decreases and the carrier concentration increases with decreasing film thickness.[36] Similar correlation between grain size and carrier concentration has been reported earlier also.[37] The grain-boundary length per unit volume appears to be playing a role in changing the carrier concentration of SnO_2 films.[36,37]

The carrier densities in the films are obtained from Hall-voltage measurements using a four-probe method (magnetic field $=5.0\times10^3$ G). A Taysurf 10 profiler (Taylor Hobson) is employed for the measurement of thickness. It gives a thickness with an accuracy of ±0.04 μm by scanning across a step on the film. The transmittance and reflectance spectra in the range 0.2–0.9 μm are obtained using a Hitachi-330 spectrophotometer.

II. THEORY

The presumed band structure of tin oxide is shown in Fig. 1 with the parabolic conduction and valence bands. The dispersions for the unperturbed bands $[E_c^0(k), E_v^0(k)]$ and for perturbed bands $[E_c(k), E_v(k)]$ are also given in the figure. The BM shift[16] is

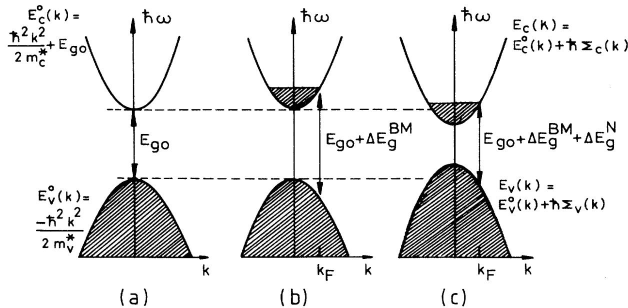

FIG. 1. (a) Schematic band structure of stoichiometric SnO_2 showing the parabolic conduction and valence bands separated by the band gap E_{g_0}, (b) after heavy doping assumed to have the sole effect of widening and band gap by a Burstein-Moss shift ΔE_g^{BM} due to filling up of the lowest states in the conduction band and (c) optical band gap as a result of the many-body interactions which partially compensate the BM widening. Shaded areas denote the occupied regions.

$$\Delta E_g^{BM} = [E_c^0(k_F) - E_v^0(k_F)] - E_{g_0} = \frac{\hbar^2 k_F^2}{2m_c^*} + \frac{\hbar^2 k_F^2}{2m_v^*} = \frac{\hbar^2 k_F^2}{2m_{vc}^*}, \tag{1}$$

where

$$m_{vc}^* = \left[\frac{1}{m_c^*} + \frac{1}{m_v^*}\right]^{-1} \tag{2}$$

is the reduced effective mass with m_c^* and m_v^* representing, respectively, the effective mass of the carriers in conduction and valence band. k_F is the Fermi wave number and is given by

$$k_F = (3\pi^2 n_e)^{1/3}. \tag{3}$$

Using (3) in (1), we have the band-gap widening ΔE_g^{BM} for carrier concentration n_e as

$$\Delta E_g^{BM} = \frac{\hbar^2}{2m_{vc}^*}(3\pi^2 n_e)^{2/3}. \tag{4}$$

Neglecting the electron-electron and electron-impurity interactions, the band gap is

$$E_g = E_{g_0} + \frac{\hbar^2}{2m_{vc}^*}(3\pi^2 n_e)^{2/3}. \tag{5}$$

A more complete theoretical model for the shifted band gaps includes the electron-electron and electron-impurity scattering. The free electrons in a degenerate material cause a downward shift of the conduction band as a result of the Coulomb interactions and mutual exchange forces between them. This shift is further accentuated by the attractive impurity scattering.[21] The influence of these interactions on the valence band causes an upward shift of the band. The ensuing effect on the optical gap is schematically shown in Fig. 1(c). The effect of various interactions can be described by the perturbed bands[21]

$$E_v(k,\omega) = E_v^0(k) + \hbar\Sigma_v(k,\omega) \tag{6}$$

and

$$E_c(k,\omega) = E_v^0(k) + \hbar\Sigma_c(k,\omega), \tag{7}$$

where $\hbar\Sigma_v$ and $\hbar\Sigma_c$ are the self-energies in the valence and conduction bands. The self-energies due to *e-e* and *e-i* interactions are assumed to be additive, i.e.,

$$\hbar\Sigma_v = \hbar\Sigma_v^{e\text{-}e} + \hbar\Sigma_v^{e\text{-}i}, \tag{8}$$

$$\hbar\Sigma_c = \hbar\Sigma_c^{e\text{-}e} + \hbar\Sigma_c^{e\text{-}i}. \tag{9}$$

The shifted optical gap, which is the measured gap, is given by

$$
\begin{aligned}
E_{gm} &= E_c(k_F,\omega) - E_v(k_F,\omega) \\
&= [E_c^0(k_F) - E_v^0(k_F)] + \hbar\Sigma_c(k_F,\omega) - \hbar\Sigma_v(k_F,\omega) \\
&= E_{g_0} + \Delta_g^{\mathrm{BM}} + \hbar\Sigma_c(k_F,\omega) - \hbar\Sigma_v(k_F,\omega) \\
&= E_{g_0} + \Delta E_g^{\mathrm{BM}} - \Delta E_g^N ,
\end{aligned} \tag{10}
$$

where

$$
\Delta E_g^N = \hbar\Sigma_v(k_F,\omega) - \hbar\Sigma_c(k_F,\omega) . \tag{11}
$$

The computations of the self-energies proceed as discussed in Ref. 17 using the random-phase approximation. The conduction band is taken to have a single valley at Γ points,[38] and is assumed to be isotropic so that $m_t = m_l$, where m_t and m_l are the transverse and longitudinal electron effective masses, respectively. A single valence band with the hole effective mass $m_{\mathrm{lh}} = m_{\mathrm{hh}} = m_v^*$ is assumed, where m_{lh} and m_{hh} represent the light-hole mass and heavy-hole mass, respectively. The static dielectric constant of the host material (ϵ) for SnO_2 is taken to be 11.5.[39,40]

The shapes of the valence and conduction bands in degenerate materials cannot be accounted for by the same effective masses as in the nondegenerate materials. Moreover, for given carrier density and effective masses, the narrowing of the band gap is not isotropic across the bands. Hence, degenerate SnO_2 is expected to have different shapes of the bands as compared to undoped stoichiometric SnO_2, i.e., we have the following.

(1) A variation of m_v^* and m_c^* with carrier density cannot be ruled out.

(2) A dependence of narrowing on k should be taken into account to have a clear idea about the shape of the bands.

The variation of m_c^* with n_e for SnO_2 films has been pointed out by many workers.[25–29] In the present studies the conduction-band effective mass m_c^* has been obtained from the optical analysis in the plasma frequency region using Drude's theory.[41] A detailed discussion is beyond the scope of the present work and is given elsewhere.[42] For the purpose of comparison, we give here a plot of the dependence of m_c^* on n_e (Fig. 2) along with the data points obtained by other workers.[25–29] As there is a scatter in the data of different workers for the same carrier concentration, a solid line is drawn to give the general trend of the variation of m_c^* with n_e for SnO_2 films. The behavior of m_c^* for carrier concentration $n_e > 6\times10^{20}$ cm^{-3} is doubtful as we have very few data points in this region. A high value of the effective mass in this region, given by the solid line, is seen to give ambiguous results while computing the total narrowing. Hence the curve of m_c^* versus n_e for lower carrier concentrations is extrapolated (dashed curve in Fig. 2) to represent the behavior of m_c^* with n_e for higher carrier concentrations. According to this curve, m_c^* varies from $\sim 0.25m_0$ for $n_e = 6.1\times10^{19}$ cm^{-3} to $\sim 0.41m_0$ for $n_e = 1.3\times10^{21}$ cm^{-3}, with most of the data points centered around $m_c^* \sim 0.3m_0$. It would not be quite unjustified if a constant m_c^* is assumed initially for simplicity.

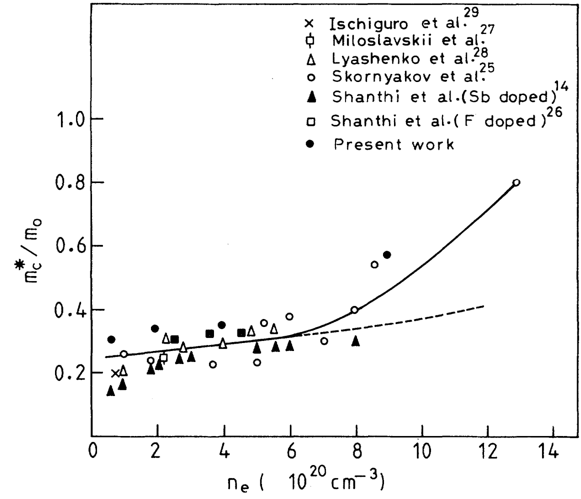

FIG. 2. Variation of the conduction-band effective mass m_c^* of SnO_2 films on carrier concentration. Data of other workers are also shown along with the present work. The dashed line is the extrapolation of the mean effective masses at lower carrier concentrations.

III. RESULTS AND DISCUSSION

The absorption coefficient, which is defined as $\alpha = 4\pi k/\lambda$, is computed from the transmittance and reflectance spectra in the fundamental absorption region. As the reflectance in the uv region is very low, the value of the absorption coefficient comes out to be the same even if the reflectance is neglected. The conventional method of obtaining the band gap in SnO_2 films is to extrapolate the α^2 versus $h\nu$ curves to $\alpha=0$; the intercept on the energy axis taken to be the band gap. Figure 3 shows such plots for a few samples having different carrier densities. The absorption edge is found to shift towards higher energies as the carrier density increases, indicating widening of the band gap with increasing carrier densities. The thickness, carrier density, and the mobility of the samples used in the present study are given in Table I.

Hamberg *et al.*,[21] however, raised some doubts about the applicability of this method for degenerate materials. Because of the widening of the initial and final states in these materials, the rise of the absorption coefficient in the fundamental absorption region is not sharp. According to Hamberg *et al.* a more accurate method of obtaining the band gap in these materials is to fit the experimentally obtained absorption coefficients to the following equation, for a given combination of E_{gm} and Γ,

$$
\alpha \propto (\Delta E_g^{\mathrm{BM}})^{1/2} \left[1 - \frac{2}{\pi} \tan^{-1} \left[\frac{E_{gm} - \hbar\omega}{\Gamma} \right] \right] , \tag{12}
$$

which in approximate form can be written as

$$
\alpha \propto 1 - \frac{2}{\pi\Gamma} (E_{gm} - \hbar\omega) . \tag{13}
$$

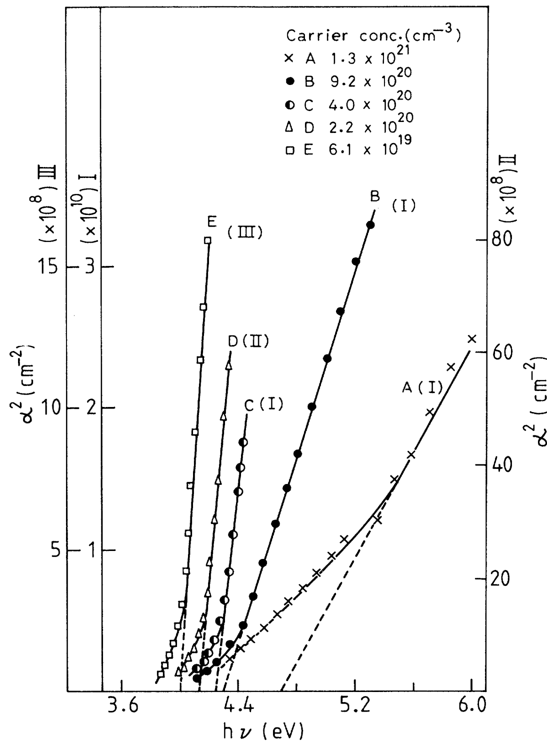

FIG. 3. Square of the absorption coefficient vs the incident photon energy for SnO_2 films of different carrier concentrations. Indicated on each plot within parentheses I, II, and III refer to the three different scales used on the α^2 axis (shown on the α^2 axis on the right and left).

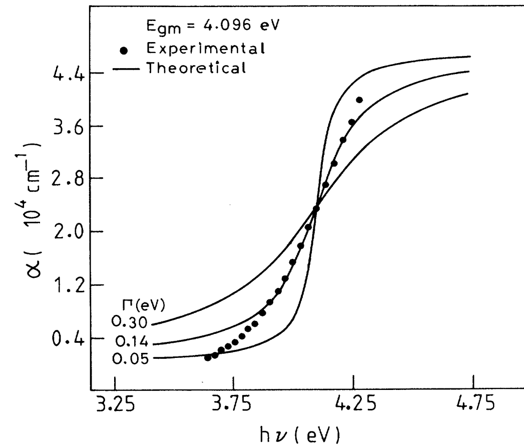

FIG. 4. Spectral absorption coefficient vs the incident photon energy for SnO_2 film. Solid circles refer to the experimentally measured data and the lines to the theoretical computations for the given E_{gm} and Γ values.

Here Γ represents the transition width. Its effect is to smear the sharp absorption edge.

In this method of curve fitting, the experimentally obtained values of α are first plotted with energy $\hbar\omega$. The above curve is expected to be steepest at the absorption edge; the steepest part thus provides the rough estimate of the value of E_{gm}. Extrapolating the linear region of the curve gives $(E_{gm} - \pi\Gamma/2)$ as the intercept on the energy axis [Eq. (13)] which gives the first approximate value of Γ. The more accurate values for E_{gm} and Γ are obtained by fitting Eq. (12) to measured values of α, taking different combinations of E_{gm} and Γ. Figure 4 shows the comparison between theory and experiment for one of the samples. Solid lines denote theoretical curves which have been fitted by selecting approximate magnitudes of E_{gm} and Γ, and solid circles correspond to the experimental points. In the above curve fitting, more weight has been given to the middle part of the curve than the tail region. Slight disagreement between the experimental and theoretical curves in the high- and low-energy side is expected due to the approximations involved in the theory.[21] It can be seen in Fig. 4 that there are only a limited number of points on the high-energy side and there is a reasonable agreement between theory and experiment. However, at the low-energy side the tailing is much more than can be accounted for by the broadening of initial and final states. This tailing at the low-energy side is possibly due to the transitions between the valence-band tail and the conduction band. The band tailing in semiconductors can arise due to various reasons, e.g., impurities, deformation potential, and dislocations, and is more for higher carrier concentration.[43] The inverse of the slope of the absorption edge, $[d(\ln\alpha)/d(h\nu)]^{-1}$, is a measure of band tailing and is expected to increase with increasing carrier concentration.[43] This is qualitatively confirmed by the behavior of the tail edges for films of different concentrations as seen in Fig. 3.

Table I gives E_{gm} and Γ as obtained from "best fits" between theory and experiment, along with the band-gap

TABLE I. The film parameters and the band gaps obtained by the extrapolation of $\alpha^2=0$ in α^2 vs $h\nu$ plots and by the curve-fitting method along with the transition width Γ.

Sample	T (μm)	n_e (cm^{-3})	μ (cm^2/V sec)	Band gap (eV) Extrapolation	Band gap (eV) Curve fitting	Transition width Γ (eV)
A	0.20	1.3×10^{21}	0.61	4.70	4.76	0.70
B	0.27	9.2×10^{20}	6.62	4.29	4.42	0.40
C	0.55	4.0×10^{20}	7.48	4.24	4.30	0.19
D	0.84	2.2×10^{20}	16.14	4.13	4.27	0.17
E	1.55	6.1×10^{19}	43.95	4.00	4.09	0.14

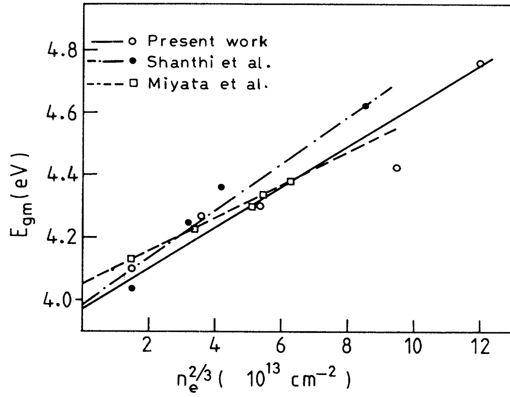

FIG. 5. The measured band gap (E_{gm}) vs $n_e^{2/3}$ for the present work (○) and Refs. 14 (●) and 12 (□).

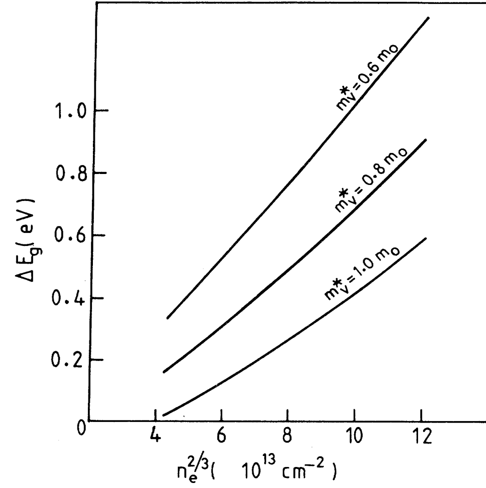

FIG. 6. ΔE_g vs $n_e^{2/3}$ computed for three magnitudes of the effective valence-band mass.

values obtained from the extrapolation method. It is seen that both E_{gm} and Γ increase as the carrier concentration increases. However, the difference between the band gaps obtained by the two methods is not always equal to Γ, as observed by Hamberg *et al.*[21] Results similar to ours have also been reported by other workers.[35,44] More studies are needed to establish a correlation between the band-gap values obtained by the two methods. Our results indicate that the conventional α^2 versus $h\nu$ plots give a reasonably good estimate of the band gap for SnO_2 films.

The experimental variation of the band gap with carrier density, n_e, in SnO_2 films has been interpreted in terms of the Burstein-Moss widening by many workers.[10–15] Ignoring the narrowing effects, the measured band gap E_{gm} at a carrier density n_e is given by [Eq. (10)]

$$E_{gm}=E_{g_0}+\frac{\hbar^2}{2m_{vc}^*}(3\pi^2 n_e)^{2/3} ,$$

where E_{g_0} is the intrinsic band gap and the second term on the right-hand side represents ΔE_g^{BM}, m_{vc}^* being the reduced effective mass.

A plot of E_{gm} versus $n_e^{2/3}$ should, therefore, give E_{g_0} as well as m_{vc}^*. Such a plot is given in Fig. 5. For the purpose of comparison, data of two other workers[12,14] are also taken and analysis on similar lines is done for them as well. From these plots, the intrinsic band gaps come out to be 3.98 eV for the present work and 4.05 and 3.96 eV for Refs. 12 and 14, respectively. The corresponding reduced effective masses are $0.59m_0$, $0.73m_0$, and $0.46m_0$, respectively. As the valence-band effective mass is given by

$$m_v^*=m_c^* m_{vc}/(m_c^*-m_{vc}^*) , \quad (14)$$

m_v^* is bound to be negative if $m_c^*<m_{vc}^*$. As seen from Fig. 2 m_c^* varies from $0.25m_0$ to $0.41m_0$ for the present study. Taking an overall average of the conduction-band effective mass as $m_c^*=0.31m_0$, m_v^* works out to be $-0.65m_0$ for the present study and $-0.54m_0$ and $-0.94m_0$ for Refs. 12 and 14, respectively.

It is presumed that the negative valence-band effective mass comes due to neglectance of narrowing. To include the narrowing of the band gap, the four self-energy terms $\hbar\Sigma_c^{e\text{-}e}$, $\hbar\Sigma_c^{e\text{-}i}$, $\hbar\Sigma_v^{e\text{-}e}$, and $\hbar\Sigma_v^{e\text{-}i}$ are computed using the expressions in Ref. 17. The self-energy terms for SnO_2 films along with the total narrowing are given in Table II. As $\hbar\Sigma_c$ comes out to be negative, the four self-energy terms are additive. Figure 6 gives plots of the theoretically computed energy-gap shift $\Delta E_g(=\Delta E_g^{\mathrm{BM}}-\Delta E_g^N)$ with $n_e^{2/3}$, for three different valence-band effective-mass values ($m_v^*=0.6m_0$, $0.8m_0$, and $1.0m_0$) taking the conduction-band effective mass $m_c^*=0.31m_0$. Here

TABLE II. The four self-energy terms contributing to the total narrowing ΔE_g^N: $m_c^*=0.31m_0$, $m_v^*=1.0m_0$.

n_e (cm^{-3})	$-\hbar\Sigma_c^{e\text{-}i}$ (eV)	$\hbar\Sigma_v^{e\text{-}i}$ (eV)	$-\hbar\Sigma_c^{e\text{-}e}$ (eV)	$\hbar\Sigma_v^{e\text{-}e}$ (eV)	ΔE_g^N
6.1×10^{19}	0.009	0.229	0.055	0.037	0.330
2.2×10^{20}	0.011	0.432	0.081	0.048	0.572
4.0×10^{20}	0.012	0.580	0.098	0.054	0.744
9.2×10^{20}	0.014	0.877	0.127	0.064	1.082
1.31×10^{21}	0.015	1.045	0.143	0.069	1.272

ΔE_g^{BM} is given by Eq. (4), and ΔE_g^N is the sum of the four self-energy terms. It is seen from the plots that increasing electron density leads to an enhanced gap shift and that for a constant carrier density, the gap shift has an inverse relationship with m_v^*.

For different combinations of m_v^* and E_{g_0}, the band gaps are theoretically computed for different carrier densities. For this purpose, the total narrowing for a given m_v^* and n_e is subtracted from the theoretical Burstein-Moss widening to give the net widening. The band gap is then given by adding this net widening to the intrinsic band gap E_{g_0}. The band gaps thus obtained for different carrier concentrations are then compared with the measured band gaps. Figure 7 shows such a comparison for two combinations of m_v^* and E_{g_0}. It is observed that $m_v^*=1.0m_0$ gives the best agreement between theory and experiment with $E_{g_0}=4.18$ eV. Figure 8 shows the self-energy contributions along with the BM widening ΔE_g^{BM} and the net shift ΔE_g in the band gap for $m_v^*=1.0m_0$. Self-energies are seen to vary approximately as $n_e^{2/3}$. The BM shift dominates the narrowing except for the low carrier concentrations.

Taking into account both the widening and the narrowing of the band gap, the corrected values of E_{g_0} and m_{vc}^* are obtained by plotting $E_{gm}+\Delta E_g^N$ [Eq. (11)] instead of E_{gm} as a function of $n_e^{2/3}$. In Fig. 9, lines (a) and (b), respectively, give the plot of $(E_{gm}+\Delta E_g^N)$ versus $n_e^{2/3}$ with and without taking narrowing into account. It is seen that inclusion of narrowing not only increases the slope of the plot but also gives an enhanced value of the intrinsic band gap. From Fig. 9, E_{g_0} comes out to be 4.18 eV which is the same as obtained from Fig. 7. Also with $m_v^*=1.0m_0$, the slope of the line (b) gives $m_0^*=0.31m_0$, which is what we started with. This way, the consistency of the obtained valence-band effective mass ($m_v^*=1.0m_0$) has been checked. It may be pointed out that the valence-band effective mass of SnO_2 obtained in the present work is higher than that estimated for indium tin oxide and ZnO (Refs. 21 and 22) using a similar procedure.

Figure 10 shows the effect of incorporating the narrow-

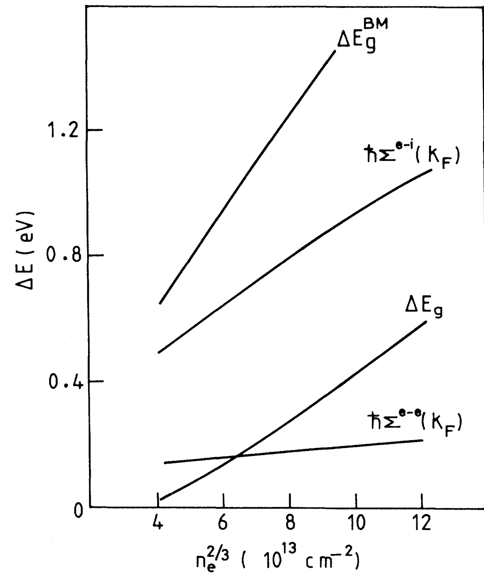

FIG. 8. The energy gap shift E_g vs $n_e^{2/3}$ computed for $m_v^*=1.0m_0$ and various contributions to E_g, i.e., from the Burstein-Moss shift (ΔE_g^{BM}), electron-impurity scattering [$\hbar\Sigma^{e-i}(k_F)$], and electron-electron scattering [$\hbar\Sigma^{e-e}(k_F)$].

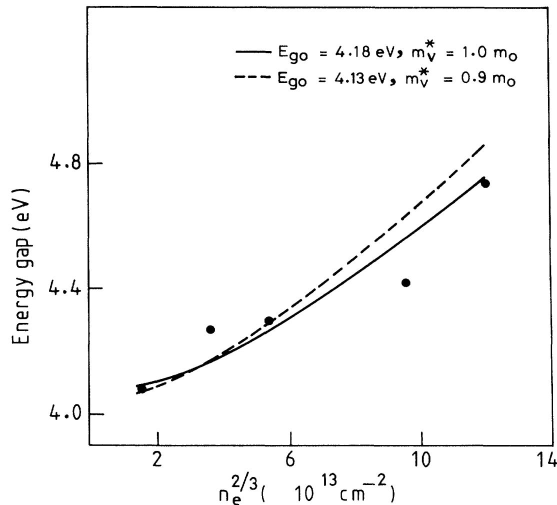

FIG. 7. Energy gap of SnO_2 films vs $n_e^{2/3}$ for different degrees of degeneracy. Solid circles represent the experimental data. Solid and dashed curves indicate the results of computations using the values shown for m_v^* and E_{g_0}. The conduction-band effective mass m_c^* is taken to be $0.31m_0$.

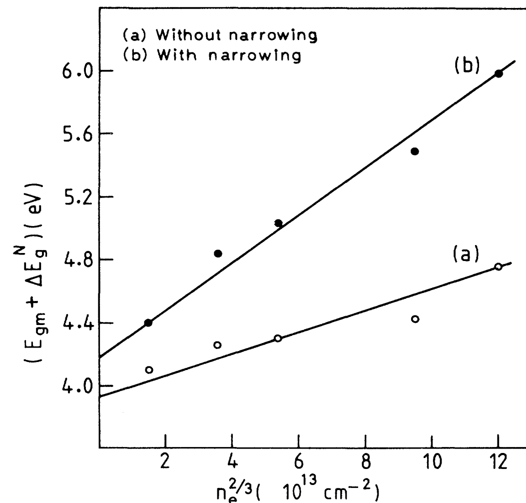

FIG. 9. $(E_{g_0}+\Delta E_g^N)$ vs $n_e^{2/3}$ showing the effect of including the narrowing on the value of the intrinsic band gap E_{g_0} and the reduced effective mass m_{vc}^*.

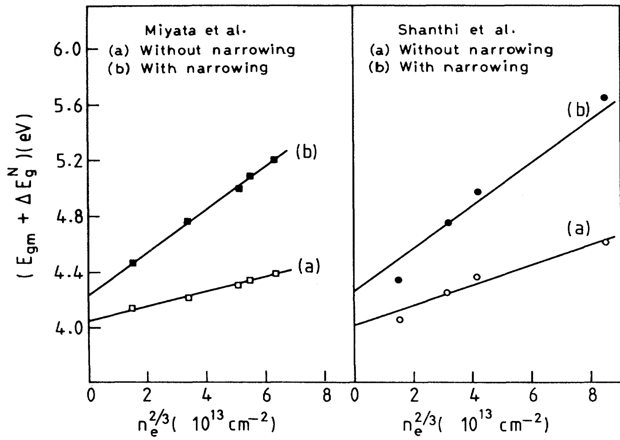

FIG. 10. $(E_{g_0}+\Delta E_g^N)$ vs $n_e^{2/3}$ showing the effect of including the narrowing on the value of the intrinsic band gap E_{g_0} and the reduced effective mass m_{vc}^* for the data from Refs. (a) 12 and (b) 14.

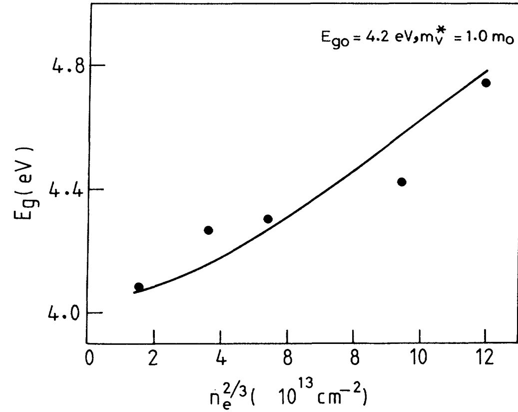

FIG. 12. Energy gap of SnO_2 films vs $n_e^{2/3}$ for different degrees of degeneracy. Solid circles represent experimental data while the solid line indicates the computed results for $E_{g_0}=4.2$ eV, $m_v^*=1.0m_0$, and taking the variations of m_c^* with carrier concentration as in Fig. 2.

ing of the band gap for the data from Refs. 12 and 14. The corrected E_{g_0} values obtained for them are 4.23 and 4.26 eV, respectively.

The variation of the actual BM shift $(\Delta E_g^{\mathrm{BM}}=E_{gm}+\Delta E_g^N-E_{g_0})$ with $n_e^{2/3}$ is shown in Fig. 11. The actual BM shift is obtained by adding the narrowing to the band gap and then subtracting the corresponding value of the intrinsic band gap from the sum. For the purpose of comparison, data points of Refs. 12 and 14 are also included. It is seen that all three data fit very well to the line of slope corresponding to $m_c^*=0.31m_0$ and $m_v^*=1.0m_0$. However, these results are based on the approximation used in taking a constant m_c^*. Taking the variation of m_c^* with n_e as given by the dashed line in Fig. 2, the self-energies are once again computed, and following the procedure already discussed, the theoretically computed band gaps are compared with the experimental values obtained from curve fitting. Again a reasonably good agreement is obtained by taking $m_v^*=1.0m_0$ (Fig. 12). This indicates that although m_c^* shows a slight variation with n_e, it can very well be assumed to have a constant value equal to $0.31m_0$ for the purpose of obtaining the value of m_v^*.

Thus, by including the many-body interactions in the valence and conduction bands, a positive value of the valence-band effective mass for SnO_2 films has been obtained, implying that the valence and conduction bands are curved in the opposite directions. With increase in the carrier density, several changes take place in the band structure. Figure 13 illustrates the dependence of the Fermi level E_F and the conduction-band minimum E_0 on

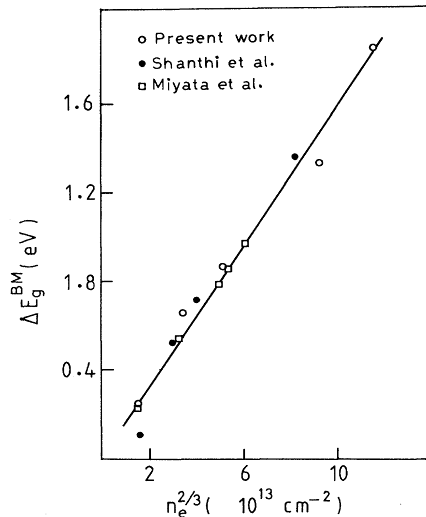

FIG. 11. The Burstein-Moss shift obtained for Refs. 14 and 12 along with the present data.

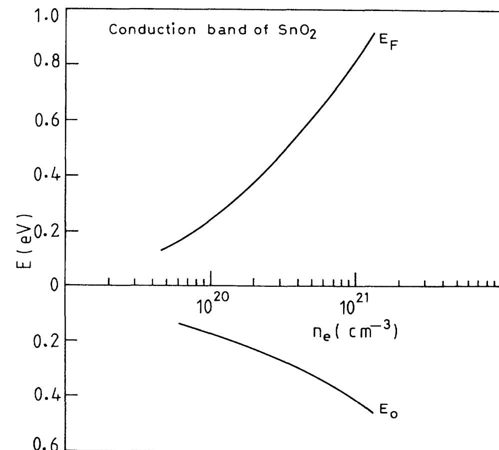

FIG. 13. Concentration dependence of the Fermi level E_F and the conduction-band minimum E_0. The reference energy is the bottom of the unperturbed conduction band.

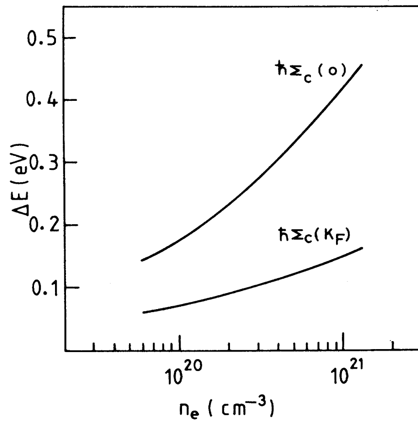

FIG. 14. The downward shift of the conduction band at $k=0$ [$\hbar\Sigma_c(0)$] and $k=k_F$ [$\hbar\Sigma_c(k_F)$]. The shift due to many-body interaction is much more at the edge of the band, i.e., at $k=0$ than at the Fermi surface, i.e., $k=k_F$.

the electron density, for degenerate SnO_2. For a degenerate material, the Fermi level is given by

$$E_F = E_{F0} + \delta E_F \tag{15}$$

Where E_{F0} corresponds to the free-electron gas and increases as $n_e^{2/3}$ and δE_F is the correction due to electron-electron and electron-impurity interactions. δE_F is simply the lowering of the conduction band at the Fermi wave number [$\delta E_F = \hbar\Sigma_c^{e\text{-}e}(k_F) + \hbar\Sigma_c^{e\text{-}i}(k_F)$]. Taking the conduction-band minimum of the stoichiometric material as the zero energy, E_0 for a degenerate material is given by the lowering of the band at $k=0$, i.e.,

$$E_0 = \hbar\Sigma_c^{e\text{-}e}(0) + \hbar\Sigma_c^{e\text{-}i}(0) \ . \tag{16}$$

With an increase in the degree of degeneracy, the Fermi level is found to move upwards whereas the conduction band clearly shifts downward.

The many body interactions in the bands not only shift the valence and conduction bands but also distort them to some degree. An attempt has been made to illustrate this distortion by comparing the downward shift of the conduction band at $k=0$ and at $k=k_F$ (Fig. 14). Clearly, the conduction band seems to be pulled down with a greater force at $k=0$ than at $k=k_F$, as $\hbar\Sigma_c(0)$ is much larger as compared to $\hbar\Sigma_c(k_F)$. This difference in the lowering at different k values results in the distortion of the bands in degenerate tin oxide.

CONCLUSIONS

The band-gap narrowing due to electron-electron and electron-impurity scattering in SnO_2 films is quite significant and cannot be neglected. The narrowing when added to experimental widening yields the actual Burstein-Moss widening and a positive valence-band effective mass $m_v^* = 1.0m_0$ is thereby obtained. This is in agreement with the proposed band structure with the valence band curved downwards and the conduction band curved upwards. Yet another consequence of taking the many-body interactions into account is that the shape of the bands gets distorted with an increase in the degree of degeneracy.

[1]C. M. Lampert, Sol. Energy Mater. **6**, 1 (1981).
[2]G. Frank, E. Kauer, and H. Kostline, Thin Solid Films **77**, 107 (1981).
[3]L. Holland and G. Siddal, Vacuum **3**, 375 (1953).
[4]K. L. Chopra, S. Major, and D. K. Pandye, Thin Solid Films **102**, 1 (1983).
[5]H. K. Müller, Phys. Status Solidi **27**, 723 (1968).
[6]Y. Ohhata, F. Shinoka, and S. Yoshida, Thin Solid Films **59**, 255 (1979).
[7]F. T. J. Smith and S. L. Lyu, J. Electrochem. Soc. **128**, 2388 (1981).
[8]S. Ray, R. Banarjee, N. Basu, A. K. Batabyal, and A. K. Barua, J. Appl. Phys. **54**, 3497 (1983).
[9]H. Nanto, T. Minami, S. Shouji, and S. Takata, J. Appl. Phys. **55**, 1029 (1984).
[10]H. Koch, Phys. Status Solidi **7**, 263 (1964).
[11]K. B. Sundaram and G. K. Bhagavat, J. Phys. D **14**, 921 (1981).
[12]N. Miyata and H. Kitahata, Thin Solid Films **125**, 33 (1985).
[13]S. Raghunath Reddy, A. K. Mallik, and S. R. Jawalekar, Thin Solid Films **143**, 113 (1986).
[14]E. Shanthi, A. Banarjee, V. Dutta, and K. L. Chopra, J. Appl. Phys. **51**, 6242 (1980).
[15]Ratnabali Banarjee and Debajyoti Das, Thin Solid Films **149**, 291 (1987).
[16]E. Burstein, Phys. Rev. **93**, 632 (1954); T. S. Moss, Proc. Phys. Soc. London Sect. **B 67**, 775 (1954).
[17]K. F. Berggren and B. E. Sernelius, Phys. Rev. B **24**, 1971 (1981).
[18]R. A. Abram, G. J. Rees, and B. L. H. Vilson, Adv. Phys. **27**, 799 (1978).
[19]G. D. Mahan, J. Appl. Phys. **51**, 2634 (1980).
[20]N. F. Mott, *Metal-Insulator Transitions* (Taylor and Francis, London, 1974).
[21]I. Hamberg, C. G. Granqvist, K. F. Berggren, B. E. Sernelius, and L. Engstrom, Phys. Rev. B **30**, 3240 (1982).
[22]Z. C. Jin, I. Hamberg, C. G. Granquist, B. E. Sernelius, and K. F. Berggren, Thin Solid Films **164**, 381 (1988).
[23]E. Shanthi, A. Banerjee, and K. L. Shopra, Thin Solid Films **88**, 93 (1982).
[24]Toshihiro Arai, J. Phys. Soc. Jpn. **15**, 916 (1960).
[25]G. P. Skornyakov and T. P. Surkova, Fiz. Tekh. Poluprovodn. **10**, 1770 (1976) [Sov. Phys.—Semicond. **10**, 1054 (1976)].
[26]E. Shanthi, V. Dutta, A. Banerjee, and K. L. Chopra, J. Appl. Phys. **53**, 1615 (1982).
[27]V. K. Miloslavski and S. P. Lyashenko, Opt. Spektrosk. **9**, 868 (1960).
[28]S. P. Lyashenko and V. K. Miloslavski, Fiz. Tverd. Tela (Len-

ingrad) **6**, 2560 (1964) [Sov. Phys.—Solid State **6**, 2042 (1964)].
[29]K. Ishiguro, T. Sasaki, T. Arai, and I. Imai, J. Phys. Soc. Jpn. **13**, 296 (1958).
[30]Geeta Sanon, Raj Rup, and A. Mansingh, Thin Solid Films **190**, 287 (1990).
[31]Debajyoti Das and Ratnabali Banerjee, Thin Solid Films **147**, 321 (1987).
[32]S. Major, A. Banerjee, and K. L. Chopra, Thin Solid Films **143**, 19 (1986).
[33]H. Kaneko and K. Miyate, J. Appl. Phys. **53**, 3629 (1982).
[34]H. Dewaal and F. Simonis, Thin Solid Films **77**, 253 (1981).
[35]Lata Gupta, A. Mansingh, and P. K. Srivastava, Thin Solid Films **176**, 33 (1989).
[36]Geeta Sanon, Ph.D. thesis, University of Delhi, India, 1990.
[37]Akira Fujisawa, Taneo Nishino, and Yoshihiro Hamakawa, Jpn. J. Appl. Phys. **27**, 552 (1988).
[38]J. Robertson, J. Phys. C **12**, 4767 (1979).
[39]R. Summit and N. F. Borroll, J. Appl. Phys. **39**, 3762 (1968).
[40]H. J. Van Daal, J. Appl. Phys. **39**, 4467 (1968).
[41]W. Steinmann, Phys. Status Solidi **28**, 437 (1968).
[42]G. Sanon, Raj Rup, and A. Mansingh (unpublished).
[43]Jaiques J. Pankove, *Optical Processes in Semiconductors* (Prentice-Hall, Englewood Cliffs, NJ, 1971), p. 43.
[44]C. V. R. Vasant Kumar and A. Mansingh, J. Appl. Phys. **65**, 1270 (1989).